INSTITUTE OF PHYSICS PUBLISHING JOURNAL OF PHYSICS: CONDENSED MATTER

J. Phys.: Condens. Matter **17** (2005) S3371–S3378 doi:10.1088/0953-8984/17/45/024

Hard sphere crystal nucleation and growth near large spherical impurities

V W A de Villeneuve, D Verboekend, R P A Dullens, D G A L Aarts, W K Kegel and H N W Lekkerkerker

Van 't Hoff Laboratory, Debye Research Institute, University of Utrecht, Padualaan 8, 3584 CH Utrecht, The Netherlands

E-mail: v.w.a.devilleneuve@chem.uu.nl

Received 28 September 2005
Published 28 October 2005
Online at stacks.iop.org/JPhysCM/17/S3371

Abstract

We report how large spherical impurities affect the nucleation and growth of hard sphere colloidal crystals. Both the impurities and the colloids are fluorescently labelled polymethylmetacrylate particles and are dispersed in an optically and density matching solvent mixture. Crystal growth, initiated either at the impurity surface, or at the sample bottom, was studied by imaging sequences of two-dimensional xy-slices in the plane of the impurity's centre of mass with a laser scanning confocal microscope. At least two factors determine whether a large impurity can function as a seed for heterogeneous nucleation: timescales and impurity curvature. The curvature needs to be sufficiently low for crystal nuclei to form on the impurity surface. If bulk crystal growth has already approached the impurity, bulk growth is dominant over growth of crystallites on the impurity surface. Such surface crystallites eventually reorient to adapt to the overall bulk crystal symmetry.

(Some figures in this article are in colour only in the electronic version)

1. Introduction

The hard sphere crystal is in many ways the simplest conceivable crystal: the hard sphere potential is infinitely repulsive at distances up to a single-particle diameter from a particle's centre and becomes zero at larger distances. The volume fraction of spheres $\phi_c = \rho v$, where ρ is the number density and v is the volume of a sphere, is therefore the only relevant parameter. This results in an athermal phase diagram [1–3], as depicted in figure 1. By embedding a single large hard sphere into a supersaturated fluid of spheres, a simple geometrical model for studying the influence of impurities on crystal nucleation and crystal growth is obtained.

The impurity/particle diameter ratio $\alpha \equiv (\sigma_i/\sigma_p)$ is a critical factor for such systems. It is well known that the presence of flat walls facilitates crystallization [4–10]. Monte Carlo

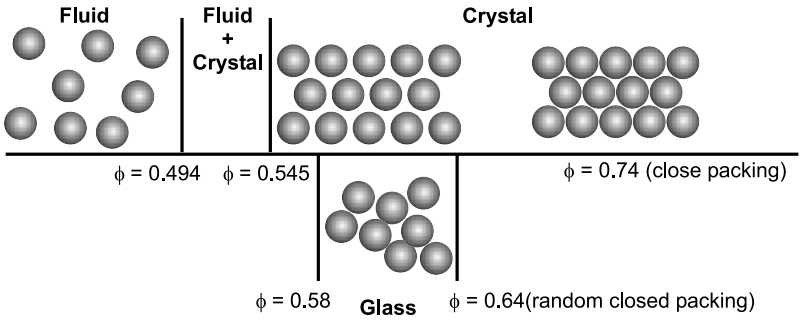

Figure 1. The hard sphere phase diagram is characterized by a fluid–crystal transition at a volume fraction of 0.494 [1]. Fluid and crystal coexist up to a volume fraction of 0.545. The non-equilibrium glassy state appears at a volume fraction of 0.58 [3].

simulations show that on hard curved impurities with $\alpha \geqslant 10$, crystal nucleation is observed in supersaturated hard sphere systems [11]. In contrast, the subsequent crystal growth stage is locally frustrated by large impurities in a system of hard spherical colloids [12], and the overall translational order in two-dimensional (2D) binary arrays of macroscopic metal balls significantly reduced [13].

Here, we study nucleation on impurities [11] and subsequent growth around the impurity, which is in competition with upward growth approaching the impurity from the sample bottom [12]. To this end we use fluorescently labelled spherical impurities and colloids in real time at the particle level using laser scanning confocal microscopy, as in e.g. [14–17]. The paper is organized as follows. In section 2 we describe our experimental system and set-up. In section 3 we describe crystal nucleation and growth (both growth from the impurity surface and upward growth from the sample bottom) near a single large impurity. In section 4 we quantify our results before we conclude in section 5.

2. Experimental system and technique

Polymethylmetacrylate (PMMA) particles, fluorescently labelled with 4-methyl amino ethylm ethacrylate-7-nitrobenzo-2-oxa-1,3-diazol (NBD), were obtained by dispersion polymerization (mass density $\rho = 1.17$ g ml^{-1}, refractive index $n_{\mathrm{D}} = 1.50$) [18]. The fluorescent dye is covalently incorporated into the polymer network of PMMA and the particles are sterically stabilized against flocculation by poly(12-hydroxystearic acid). A set of 6% polydisperse 1.5 μm particles was mixed with a small amount (up to 1 wt%) of very polydisperse (3–45 μm diameter) particles to obtain a system of monodisperse particles contaminated with a small amount of impurities of varying sizes. The particles are dispersed in a density and optically matching apolar solvent mixture of *cis*-decalin (Merck, for synthesis, 30% v/v), tetralin (Merck, for synthesis, 35% v/v) and tetrachloromethane (Merck, for spectroscopy, 35% v/v), similarly to in [19]. The use of an optically matching apolar solvent mixture ($\Delta n_{\mathrm{D}} \approx 0.0050$) results in hard sphere interactions. The low density difference (1.16 g ml^{-1}; density difference $\Delta\rho \approx 0.01$ g ml^{-1}) between the solvent and the particles gives a relatively large gravitational length of $\sim$23 μm.

Thin 2D cross sections of the sample were imaged with a Nikon Eclipse TE2000U laser scanning confocal microscope with a Nikon C1 scanning head in combination with an argon laser ($\lambda_0 = 488$ nm), and an oil-immersion lens (Nikon Plan APC 100X, NA 1.4). The $\sim$0.3 ml samples were stored in small vials. The bottom of the vial was removed and replaced by a

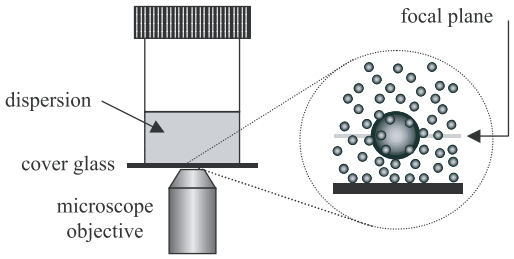

Figure 2. Experimental set-up. Samples are imaged in the horizontal plane of the impurity's centre of mass. The focal plane is set up at 40 μm above the sample bottom.

Table 1. Details of the recorded confocal image sequences.

α	ϕ_c	h (μm)	Figure	Impurity conc. (wt%)
13	0.55	15	3(A)	0.1
27	0.54	25	3(B), 4, 5	1
17	0.54	42	3(C)	1

microscope cover glass (Chance Propper Ltd, West Midlands, UK, 0.11 mm thickness), which was glued to the vial using an epoxy glue (Araldit AW2101) with hardener (HW2951). The sample weight was checked regularly to monitor the solvent evaporation, which was negligible.

In this work, we imaged the particles present at distances of 15–40 μm from the glass sample bottom (sample heights h), parallel to the flat sample bottom. The particle polydispersity (6%) blows up homogeneous nucleation timescales [4] and up to 25 μm from the wall only heterogeneous nucleation at the sample bottom and subsequent upward growth is observed [12]. Upward growth from the sample bottom is therefore solely characterized by the (111) plane, which enables investigation of crystal growth by inspecting the hexagonal order. By choosing a high volume fraction $\phi_c = 0.54$–0.55—determined relative to the random packing density 0.66 [20]—the impurities become positionally locked in the crystal, which grows upward. Growth around the impurity can thus be studied over several hours with little impurity movement. Heterogeneous nucleation on impurities can be studied before upward crystal growth approaches the field of view. Confocal image sequences were recorded in the horizontal plane of the impurity's centre of mass, as shown schematically in figure 2. Details of all sequences are given in table 1.

3. Crystallization near a single impurity

In figure 3, representative confocal images of crystallization near large spherical impurities are shown. Figure 3(A) depicts crystal growth near a single impurity with $\alpha = 13$. On average, crystal growth takes place earlier further away from the impurity. Close to the impurity the system remains relatively unordered, and a persisting single-particle fluid layer is observed on the impurity surface. Only upward crystal growth towards the impurity surface, no heterogeneous nucleation onto the surface is observed.

Moving on to a larger spherical impurity ($\alpha = 27$) we clearly see a different phenomenon. On the impurity surface, approximately three layers form (figures 3(B1) and (B2)) before crystal nuclei start to grow away from the impurity (figure 3(B3)). The fluid layer clearly does not persist as curvature is decreased beyond the minimum studied in [12]. Apart from the varying orientations along the surface of the impurity, a series of images at different distances

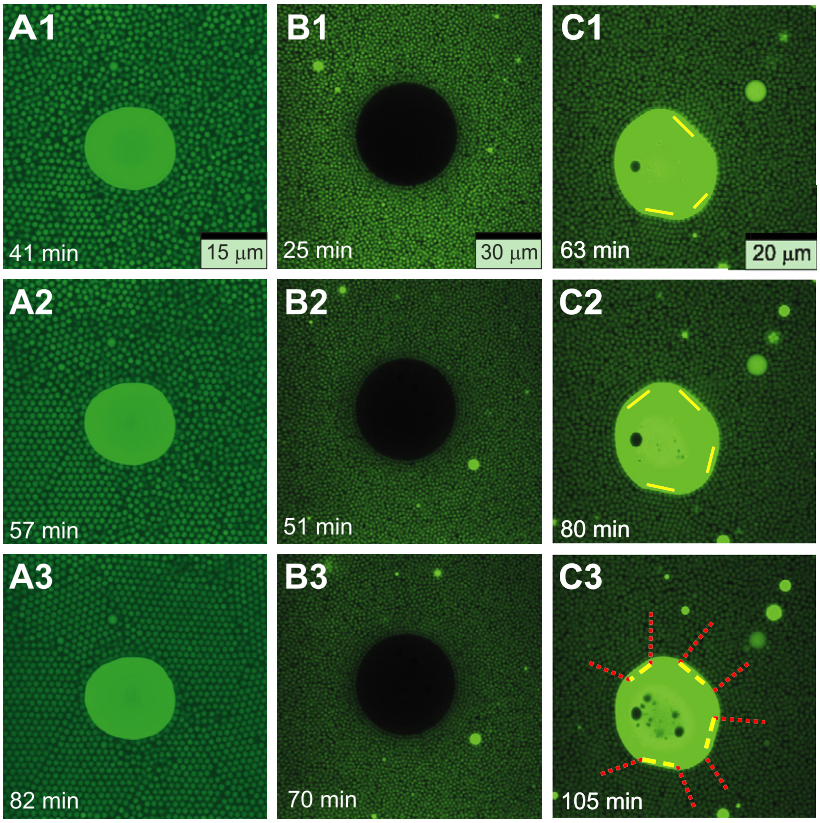

Figure 3. Confocal images of crystallization. (A) Crystal growth near an impurity ($\alpha = 13$). Crystal growth in the field of view sets in far away from the impurity and approaches it. (B) Crystal nucleation on an impurity with $\alpha = 27$. Crystal nucleation takes place on the impurity surface before upward growth from the sample bottom reaches the field of view. Note that the impurity is much less fluorescent than most other impurity particles, but does share the refractive index and structure with holes with the other large impurities present. (C) Crystal growth on an impurity with varying curvature. Crystallites have nucleated on the less curved parts (the dashed lines indicate where crystallites grow on the impurity surface); the dotted lines in (C3) mark the crystallites grown.

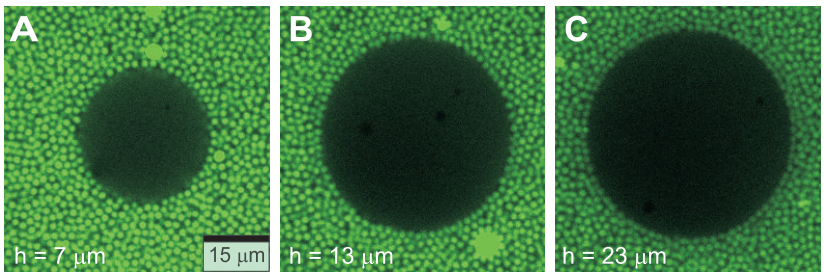

Figure 4. Confocal images taken after 21 min at different sample heights show that no upward crystal growth close to the impurity is observed shortly before nucleation is initiated.

from the sample bottom clearly show that nucleation, not crystal growth, is observed initially along the impurity surface (figure 4).

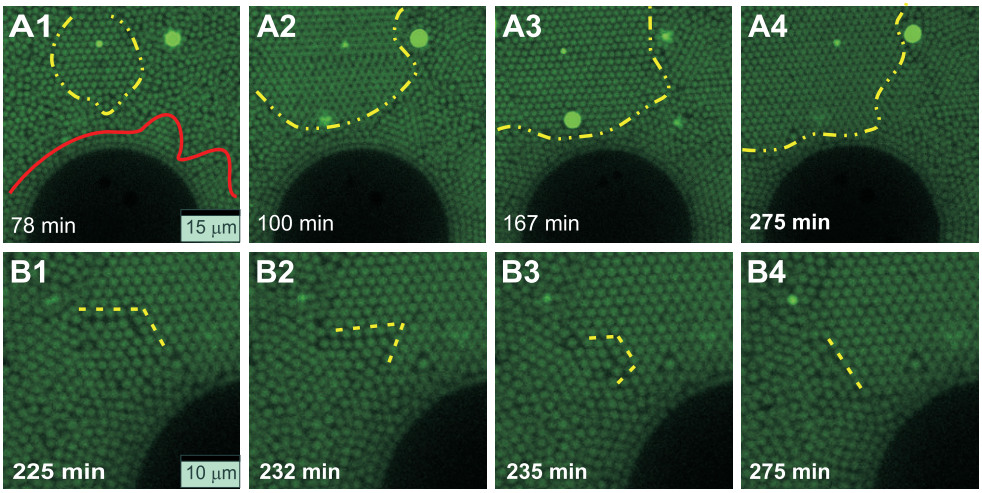

Figure 5. Late stages of crystallization near an impurity with $\alpha = 27$. (A) Crystal growth from the bottom starts in the field of view and the crystallites on the impurity surface reorient to the bulk crystal orientation (dark line: crystallites on the impurity surface; dotted lines bulk crystal). (B) Growth from the bottom appears in the field of view and crystallites formed on the impurity surface adjust their position to the bulk crystal. The dotted lines mark the grain boundary translation by which surface crystallites reorganize to the crystal's symmetry.

Pure serendipity permitted us to investigate the influence of local impurity curvature on heterogeneous nucleation even more directly by studying crystallization near an impurity with varying curvature (figure 3(C)). At the start of the recorded confocal image sequence, nucleation has already initiated on this impurity with $\alpha = 17$ (figure 3(C1)). Crystal nuclei have clearly formed on the less curved parts of the impurity and grow away from the impurity (figure 3(C3)). Where curvature is high on the impurity surface, the disordered fluid phase is predominantly observed. This confirms that local impurity curvature, not impurity size, determines whether an impurity can function as a seed for heterogeneous nucleation.

Crystallization near the $\alpha = 27$ was imaged up to much longer timescales (figure 5(A)). After ~70 min, upward crystal growth reaches the field of view, with the clear (111) orientation in the horizontal plane. Due to the impurity curvature, grain boundaries, directed towards the impurity, separate the various crystallites on the impurity surface. Growth from the impurity surface stops when a grain boundary is formed with the approaching crystal front of the bulk crystal. The crystallites that have formed on the impurity surface reorganize afterwards to adapt to the bulk crystal's symmetry (figure 5).

4. Analysis

To quantify the impurity's effect on local crystallization we use the local orientational bond order parameter ψ_6 [21]:

$$\psi_6(\vec{r}) = \frac{1}{N}\sum_{j}^{N} \mathrm{e}^{6\mathrm{i}\theta(\vec{r}_j)}, \tag{1}$$

where $\psi_6 \approx 0.4$ for a typical fluid and $\psi_6 = 1$ for a perfect 2D hexagonal crystal. The summation j runs over all N next neighbours of a given particle. The angle between the bond vector connecting the particle with its next neighbour j and an arbitrary fixed reference axis

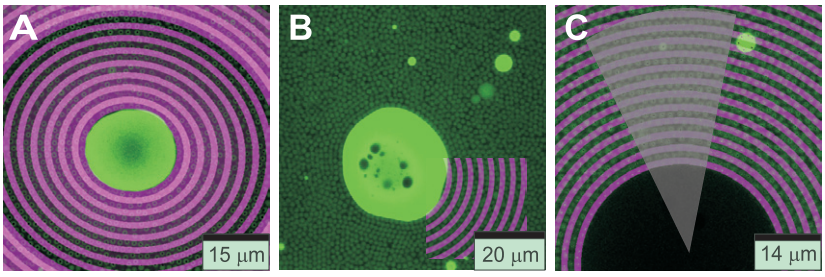

Figure 6. (A) Particles are divided into shells around the impurity to obtain a time and distance dependent crystallization profile. (B, C) For the heterogeneous nucleation image sequences a small section of the image is considered for analysis, where the (111) plane is parallel to the sample bottom. For (B), the square in which the shells are shown was considered for analysis. In (C), the shaded area is the area considered for analysis. Shells of 1.5 μm thickness are shown in all cases.

is defined as $\theta(\vec{r_j})$. Particle coordinates are obtained using methods such as that in [22]. The minimal translation and rotation of the impurity are tracked as well.

For crystal growth near impurities and crystal nucleation on impurities, particles are divided into shells around the impurity, based on the distance to the impurity's surface. Averaging over all particles of shell s, its hexagonal order parameter $\langle|\psi_6|\rangle_s$ is obtained, which is used to obtain a time dependent crystal growth profile per shell (figure 6).

Typical crystal growth profiles of shells of 5.0 μm thickness around the impurity with $\alpha = 13$ are shown in figure 7(A). All shells start crystallizing simultaneously. The shells evolve from a fluid $\langle|\psi_6|\rangle_s \approx 0.4$ into a more crystalline $\langle|\psi_6|\rangle_s \approx 0.8$, where $\langle|\psi_6|\rangle_s$ plateaus. A constant $\langle|\psi_6|\rangle_s$ value is not reached for the first shell during the image sequence. Crystal growth clearly proceeds more rapidly further away from the impurity. The scenario should be the same if growth is not initiated heterogeneously at the flat sample bottom, but homogeneously in the bulk.

To analyse the nucleation on spherical impurities, selections of the image were analysed where the crystal's (111) plane was parallel to the field of view (figure 6(B)). The $\langle|\psi_6|\rangle_s$ values of the image series of the impurity with varying curvature (figure 3(C)) were obtained by averaging over ten images as well. Averaging enables us to show the observed trends more clearly by suppressing the relatively large fluctuations and errors in particle positions in such small data sets. For similar reasons, the $\langle|\psi_6|\rangle_s$ values of the image series in figure 3(B) were averaged over ten images as well.

Growth of crystallites on the impurity with varying curvature clearly takes place earlier close to the impurity (figure 7(B)) after which layer by layer growth is observed. This agrees with our experimental observations (figure 3(C)), but is in sharp contrast to figure 7(A) and proves that two very different scenarios are observed.

A similar trend is seen on the impurity with $\alpha = 27$ (figure 7(C)): increase of order takes place earlier at 1.5–3.0 μm than at 3.0–4.5 μm, which confirms the scenario of nucleation on and growth away from the impurity. At 5–10 μm, no increase in order is observed during the time sequence, but at 10–15 and 150–20 μm sharp increases in local order are observed when upward growth reaches the field of view. The graph also shows that increase of order further away from the impurity takes place later, when the crystal grows upward from the bottom. The reorientation of the crystallites on the impurity and therefore also the displacement of the grain boundary towards the impurity coincides with a decrease in local order close to and an increase of local order far from the impurity. Bulk growth is clearly predominant over growth from nuclei on curved surfaces when these two compete locally.

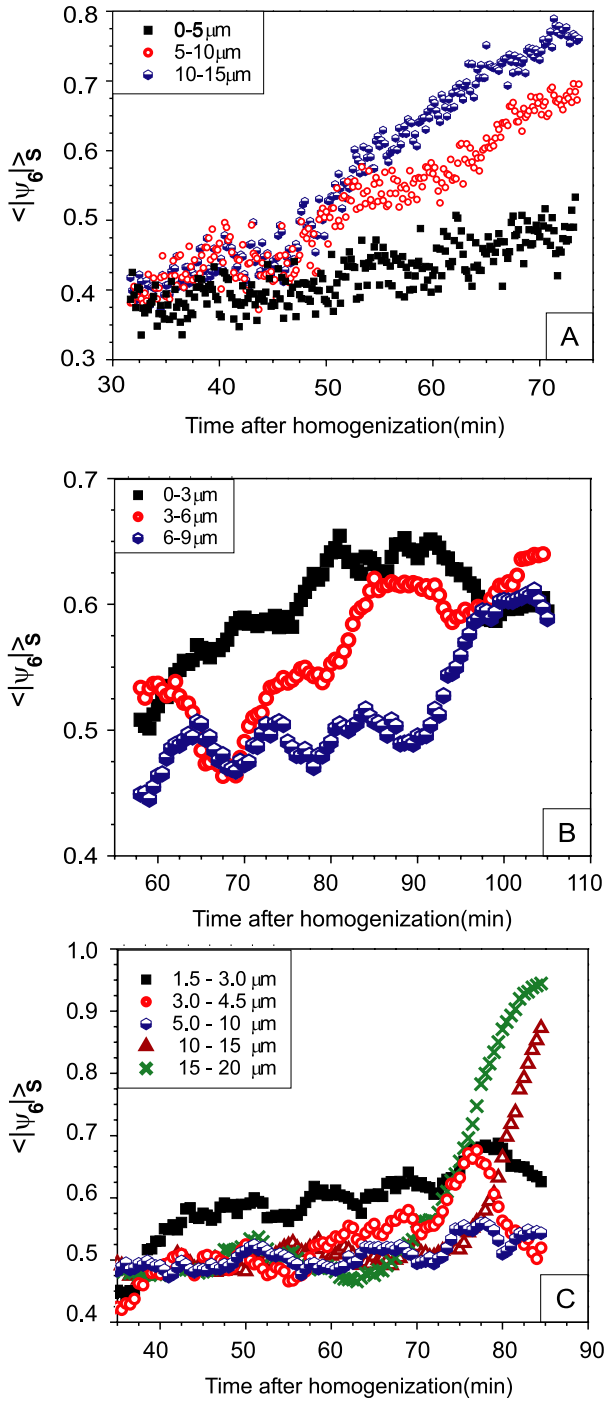

Figure 7. Quantitative analysis. (A) Around an impurity with $\alpha = 13$, crystal growth proceeds more slowly close to the impurity. (B) On an impurity with varying curvature, crystallite growth starts earlier close to the impurity than further away. (C) On an impurity with $\alpha = 27$, crystallite growth proceeds earlier close to the impurity. The approach of the crystal front towards the impurity coincides with the local decrease in $\langle|\psi_6|\rangle_6$ in the 1.5–3.0 μm and 3.0–4.5 μm shells after $\sim$80 min.

5. Conclusion

We show that two main factors control whether an impurity can function as a seed for heterogeneous nucleation in hard sphere crystals: curvature and timescales. If the surface's curvature is high, no nucleation takes place, and a single-particle-thickness fluid layer persists on the impurity surface. Nucleation (and therefore the onset of at least a single crystalline layer) occurs preferably on less curved surfaces, as observed on the surface with varying curvature. If bulk crystal growth has already set in close to the impurity, it will be the predominant process, and crystallites formed due to heterogeneous nucleation will adjust their orientation to the bulk crystal. Quantitative analysis confirms that two very different scenarios are observed: (I) upward crystal growth which proceeds more slowly close to the impurity and (II) crystal nucleation on the impurity surface and subsequent growth away from it. Therefore the observed persisting fluid layer on impurities, approached by a growing crystal front [12], and the nucleation of hard sphere crystals at curved impurity surfaces [11] agree perfectly with each other.

Acknowledgments

Gilles Bosma, Hans Scherff and Esther Groeneveld are acknowledged for particle synthesis. The work of VWAdV is part of the research programme of the Stichting voor Fundamenteel Onderzoek der Materie (FOM), which is financially supported by the Nederlandse Organisatie voor Wetenschappelijk Onderzoek (NWO). Support of VWAdV by the DFG through the SFB TR6 is acknowledged.

References

[1] Alder B J and Wainwright T E 1957 *J. Chem. Phys.* **27** 1208
[2] Pusey P N and van Megen W 1986 *Nature* **320** 340
[3] Pusey P N and van Megen W 1987 *Phys. Rev. Lett.* **59** 2083
[4] Auer S and Frenkel D 2003 *Phys. Rev. Lett.* **91** 015703
[5] Kose A and Hachisu S 1976 *J. Colloid Interface Sci.* **55** 487
[6] Gast A, Russel W and Hall C 1986 *J. Colloid Interface Sci.* **55** 161
[7] Kaplan P D, Rouke J L, Yodh A G and Pine D J 1994 *Phys. Rev. Lett.* **72** 582
[8] Dinsmore A, Warren P, Poon W and Yodh A 1997 *Europhys. Lett.* **40** 337
[9] Martelozzo V C, Schofield A, Poon W C K and Pusey P N 2002 *Phys. Rev.* E **66** 021408
[10] Dullens R P A and Kegel W K 2004 *Phys. Rev. Lett.* **92** 195702
[11] Cacciuto A, Auer S and Frenkel D 2004 *Nature* **428** 404–6
[12] de Villeneuve V W A, Dullens R P A, Scherff E, Aarts J H, Groeneveld D G A L, Kegel W K and Lekkerkerker H N W 2005 *Science* **309** 1231–3
[13] Nelson D R, Rubinstein M and Spaepen F 1982 *Phil. Mag.* A **46** 105–26
[14] van Blaaderen A and Wiltzius P 1995 *Science* **270** 1177
[15] Kegel W K and van Blaaderen A 2000 *Science* **287** 290–3
[16] Pham K N, Puertas A M, Bergenholtz J, Egelhaaf S U, Moussaid A, Pusey P N, Schofield A B, Cates M E, Fuchs M and Poon W C K 2002 *Science* **296** 104–6
[17] Schall P, Cohen I, Weitz D A and Spaepen F 2004 *Science* **305** 1944–8
[18] Bosma G, Pathmamanoharan C, de Hoog E H A, Kegel W K, van Blaaderen A and Lekkerkerker H N W 2002 *J. Colloid Interface Sci.* **245** 292–300
[19] de Hoog E H A 2001 Interfaces and crystallization in colloid–polymer suspensions *PhD Thesis* Utrecht University
[20] Schaëtzel K and Ackerson B J 1994 *Phys. Scr.* T **49** 70
[21] Nelson D R 2002 Statistical mechanics of two-dimensional melting *Defects and Geometry in Condensed Matter Physics* (Cambridge: Cambridge University Press) pp 68–91
[22] Crocker J C and Grier D G 1996 *J. Colloid Interface Sci.* **179** 298–310